Impact ionization in high resistivity silicon induced by an intense terahertz field enhanced by an antenna array

Tarekegne, Abebe Tilahun; Iwaszczuk, Krzysztof; Zalkovskij, Maksim; Strikwerda, Andrew; Jepsen, Peter Uhd

Published in:
New Journal of Physics

Link to article, DOI:
10.1088/1367-2630/17/4/043002

Publication date:
2015

Document Version
Publisher's PDF, also known as Version of record

Impact ionization in high resistivity silicon induced by an intense terahertz field enhanced by an antenna array

2015 New J. Phys. 17 043002

(http://iopscience.iop.org/1367-2630/17/4/043002)

New Journal of Physics
The open access journal at the forefront of physics

Deutsche Physikalische Gesellschaft DPG
IOP Institute of Physics

Published in partnership with: Deutsche Physikalische Gesellschaft and the Institute of Physics

OPEN ACCESS

RECEIVED
3 February 2015

ACCEPTED FOR PUBLICATION
3 March 2015

PUBLISHED
2 April 2015

PAPER

Impact ionization in high resistivity silicon induced by an intense terahertz field enhanced by an antenna array

Abebe T Tarekegne, Krzysztof Iwaszczuk, Maksim Zalkovskij, Andrew C Strikwerda and Peter U Jepsen

Department of Photonics Engineering, Technical University of Denmark, Ørsteds Plads, Building 344, DK-2800 Kgs. Lyngby, Denmark

E-mail: atil@fotonik.dtu.dk

Keywords: impact ionization, THz filed, antenna array, silicon

Abstract

We report on the observation of ultrafast impact ionization and carrier generation in high resistivity silicon induced by intense subpicosecond terahertz transients. Local terahertz peak electric fields of several MV cm^{-1} are obtained by field enhancement in the near field of a resonant metallic antenna array. The carrier multiplication is probed by the frequency shift of the resonance of the antenna array due to the change of the local refractive index of the substrate. Experimental results and simulations show that the carrier density in silicon increases by over seven orders of magnitude in the presence of an intense terahertz field. The enhancement of the resonance shift for illumination from the substrate side in comparison to illumination from the antenna side is consistent with our prediction that the back illumination is highly beneficial for a wide range of nonlinear processes.

1. Introduction

Impact ionization is a carrier multiplication mechanism where energized conduction band electrons collide with bound electrons to generate new electron-hole pairs [1–3]. Impact ionization can generate a significant population of free carriers through a cascade of collision processes in the presence of an external force. Terahertz (THz) pulses have been used for carrier multiplication in low-bandgap and direct-bandgap semiconductors [1, 4]. Employing ultrashort electric field pulses for impact ionization enables switching of the conductivity of semiconductors on an ultrafast time scale. The investigation of such an immense carrier generation potential has been limited in silicon to theoretical simulations with experimental verifications based on strong static electric fields [2, 5–7]. A pure optical, noncontact and ultrafast impact ionization technique enables a better understanding of ultrafast carrier dynamics in silicon and it increases its functionality. We foresee applications of such ultrafast carrier multiplication in integrated circuit technology, metamaterial and antenna design.

THz technology is advancing rapidly thanks to development of ultrafast high power lasers and substantial improvements in THz generation and detection schemes. It has recently become possible to generate intense THz fields on order of MV cm^{-1} [8–14]. Such strong THz electric fields provide new means of investigation and control of carrier dynamics in semiconductors [15–19]. THz pump-probe time domain spectroscopy has recently been used to study impact ionization in a low-bandgap semiconductor (indium antimonide, InSb [4] and indium arsenide, InAS [20]) and in a direct semiconductor (gallium arsenide, GaAs) [1]. Here we report free carrier multiplication in an indirect bandgap material, silicon, induced through a cascade of impact ionization events. Impact ionization in silicon requires a strong driving force owing to its indirect bandgap [7, 21]. Other competing processes, such as phonon scattering and intervalley scattering, eclipse impact ionization for insufficient electric fields [5, 22]. The required THz peak electric field is so high that our THz source alone is not capable of inducing measurable carrier multiplication. For that reason we further enhance the THz field strength by utilizing nearfield enhancement of the field provided by a metallic antenna array. Results presented in this paper are of particular importance for various THz devices fabricated on silicon at high THz field strength [23–25].

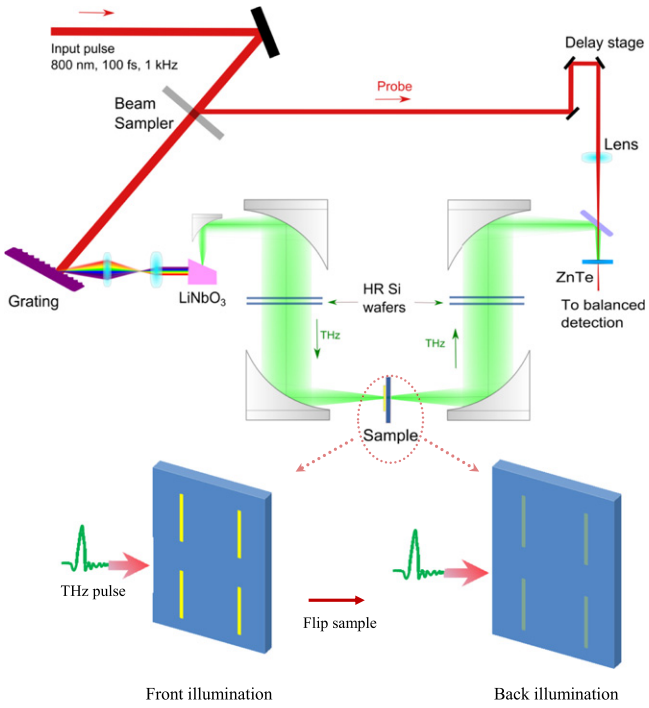

Figure 1. Schematic diagram of the experimental setup. A 800 nm laser pulse from a regenerative Ti:sapphire amplifier generates THz transient in $LiNbO_3$ crystal. The THz pulse is collimated and focused at the sample location using a set of off-axis parabolic mirrors. The transmitted THz signal is imaged onto ZnTe crystal where it overlaps with the probe pulse for THz detection. The sample is illuminated either from the antenna side (front illumination) or from the substrate side (back illumination).

2. Methodology

A nearly single cycle THz field is generated by optical rectification in a lithium niobate ($LiNbO_3$) crystal in a tilted wavefront geometry [26–28] by 800 nm pulse from a Ti:sapphire regenerative amplifier (Spitfire Ace). The laser pulses from the amplifier have energy of up to 6 mJ, a pulse width of 100 fs and a repetition rate of 1 kHz. The near infrared (NIR) beam is separated into two parts using an optical sampler. The major portion of the beam which passes through the optical sampler is used for THz generation and a small fraction of the beam is used as a probe beam for the THz electric field measurement. In the optical rectification method, the NIR laser pulse front is tilted using a diffraction grating to achieve phase matching in the lithium niobate crystal. The THz beam is then collimated and focused at the sample location using a set of 90° off-axis parabolic mirrors (see figure 1).

The THz signal propagates through the sample and is imaged by another set of off-axis parabolic mirrors on a ZnTe crystal for THz pulse detection. The detection mechanism is based on free space electro-optic sampling in a 0.5 mm thick <110> ZnTe crystal [29–31]. The THz field strength is estimated from the THz induced phase retardation of the probe beam in the detection crystal due to the linear Pockel's effect in a balanced detection system. To avoid over rotation and any nonlinearities [32, 33] in the electro-optic detection, we decrease the intensity of THz wave on the ZnTe crystal by inserting a set of nine high resistivity (HR) Si 525 μm thick wafers in the path of the collimated THz beam, resulting in a field strength reduction by a factor of $(0.7)^{-0.9} = 24.8$. The silicon wafers are also used to vary the THz field strength at the sample location by relocating the HR Si wafers in the THz beam path before and after the sample. The total number of HR Si in the beam path is kept constant to maintain a constant THz field strength at the detector.

By scanning the time delay between the THz beam and the detection beam, a time domain THz field waveform is mapped out as shown in figure 2. The THz pulse has peak field strength >250 kV cm^{-1} as measured by electrooptic sampling. The inset in figure 2 shows the amplitude spectrum obtained by calculating the fast Fourier transform of the time domain pulse. The experiments are conducted at room temperature unless otherwise noted, and in a dry atmosphere maintained by a dry nitrogen purge.

To achieve an electric field sufficient for impact ionization in silicon, we fabricate periodic gold antenna arrays on HR Si substrates by means of standard UV lithography. It is well known that metal antennas fabricated on top of a dielectric substrate can provide significant local field enhancement [34, 35]. A scanning electron microscope image of a gold antenna array with a resonant frequency of 0.6 THz is shown in figure 3(a). The calculated field profile for a single antenna unit excited by a plane wave source with a temporal profile depicted in

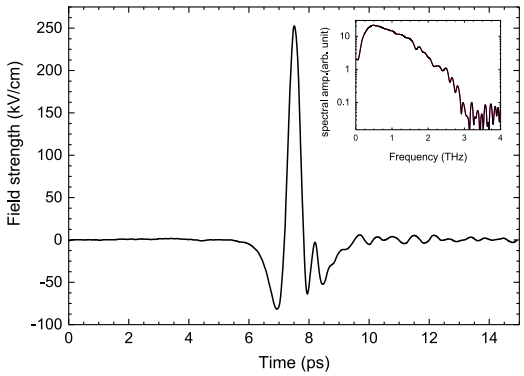

Figure 2. THz transient generated by optical rectification in $LiNbO_3$ measured at the sample position. The inset shows the corresponding amplitude spectrum.

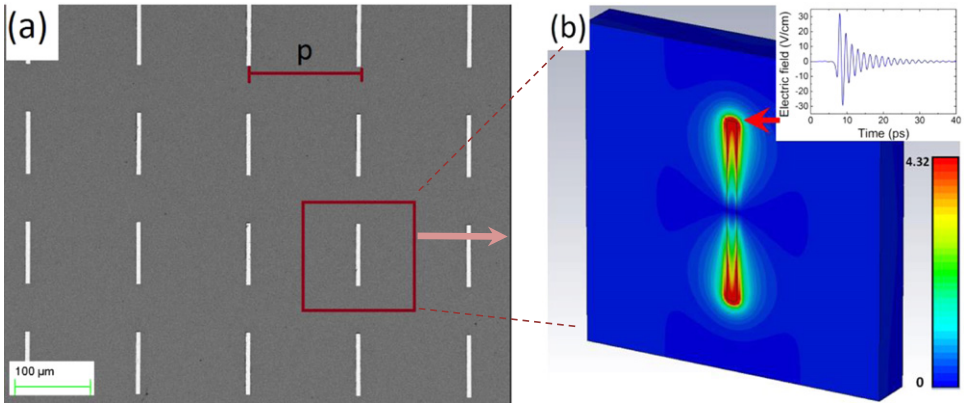

Figure 3. (a) Scanning electron microscope image of a periodic gold antenna array designed for a resonance frequency at 0.6 THz. (b) Simulated time domain THz electric field profile in the vicinity of a single antenna unit. The antenna has a length of 80.6 μm, a width of 5 μm and a thickness of 200 nm. The periodicity of the antenna array in both directions is 143.8 μm. The inset shows the magnitude of electric field at the tip of an antenna for an incident plane wave with peak electric field of 1 V m^{-1}.

figure 2, is calculated by a commercial full-wave electromagnetic solver is shown in figure 3(b). The color scale is limited to only 4.32 at the peak of the response in time domain in spite of a maximum field enhancement of ~30 to better visualize the field profile near the antenna. In the modeling of the antenna array the dimensions are set according to the measurements of the fabricated sample. Periodic boundary conditions are implemented in the *x*- and *y*- directions to represent the periodic antenna arrays while considering a single antenna for simulations. A lossy metal with electrical conductivity of 4.561×10 S m^{-1} is used to model the optical constants of gold. The real part of dielectric constant of silicon is set to be 11.7 as specified by the supplier (Topsil) and in agreement with literature in the THz range [36]. Simulation results show that the field is enhanced by more than 30 times in the time domain near the top and bottom tips of the antenna at the depth of 0.01 μm in the silicon substrate, see figure 3(b) inset.

3. Results and discussions

We measure THz transmission of the antenna array for several incident THz field strengths and show results on figure 4. To obtain the transmission spectrum of the antenna array, we divide the Fourier transform of the transmitted THz transient through the sample by that of a bare HR Si reference. We note here that we do not observe any measurable change of transmission through bare HR Si even at highest available field strengths. Transmission spectrum through the antenna array exhibits a broad resonance centered at 0.6 THz. The width of observed resonance is limited by the width of the time domain window of our measurement, which in turn is limited by arrival of Fabry–Perot reflections from the sample, detection crystal and silicon wafers. We set the time measurement window to 15 ps and this time window is used in subsequent simulations. The resonance frequency of the antenna red-shifts and slightly broadens with increasing THz field strength as shown in figure 4.

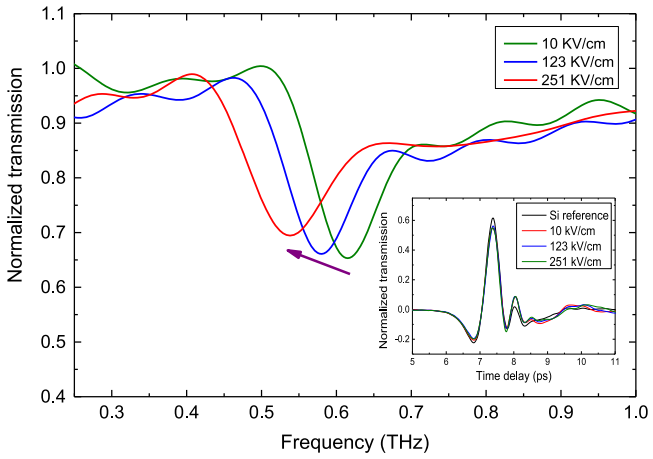

Figure 4. Measured THz transmission of a gold antenna on a high resistivity silicon substrate as a function of frequency for different incident THz peak field strengths. The arrow indicates direction of increasing THz field strength. Transmission is normalized to transmission through a bare HR Si wafer. The inset shows the transmitted THz transient for several incident THz field levels.

To exclude the possibility that the resonant frequency shift is caused by changes to the metal antenna itself, we performed the same experiment for an antenna array fabricated on insulating fused silica glass. As expected, no shift of the resonant frequency has been observed in that case, even at highest achievable field strengths. At the tips of the antenna, the field strength is sufficient for THz-induced field emission of electrons in to the surrounding atmosphere as we recently reported [23].

We attribute the change of the resonance frequency to a change of optical properties of the substrate induced by strong THz field. Antenna theory predicts the approximate value of a resonant frequency f_{res} of an antenna to be $f_{res} = c/(2n_{eff}L)$, where L is length of the antenna; c is the speed of light and n_{eff} is the effective refractive index of the substrate [34]. According to this model, an increase of the effective refractive index of the substrate will result in the redshift of the resonant frequency. An accurate evaluation of the refractive index change of the substrate in our case is not straight forward since its local value depends on the local THz electric field in a nonlinear manner.

The change in transmission resonance frequency with refractive index is reproduced with full-wave simulations by modifying the refractive index of HR Si locally in the vicinity of the antenna tips. We arbitrarily limit that volume to the region where the peak THz field strength is larger than a certain threshold value E_{th}. To maintain consistency with the measurements, a measured THz transient is used as an input in the simulation and the solver duration is also kept at the same length as the measurement time window (15 ps). In order to keep the simulation tractable we assume that the refractive index change is constant if the field strength is greater than the threshold value E_{th} and negligible in the substrate regions with THz electric field smaller than the threshold. We use a Drude model to analyze the dielectric properties of the substrate near antenna tips with parameters adopted from Willis *et al* [37]. Even though it is difficult to determine the local refractive index change, we can still determine the average refractive index change of the substrate near the antenna tips. Figure 5 shows transmission spectra simulated with various refractive index changes that correspond to same shift as measurements from figure 4. Our simulations show that the average refractive index in the vicinity of the antenna needs to increase by 4 to match the resonant frequency shift measured in the experiments for an input field of 251 kV cm^{-1}. The imaginary part of the refractive index also changes in the vicinity of the antenna tips. However, our simulations show that change of only the imaginary part of the refractive only does not result in a shift of the antenna resonance frequency and it is not discussed in detail in this article.

Comparing figures 4 and 5 we clearly see that the transmission spectra of the antenna array are well reproduced by the simulations. Our measurements show that at high electric field the transmission resonance is slightly broader and the resonance is not as strong as low electric field resonance. We do not observe this behavior in our simulations. This is expected in the simulations since we use a uniform plane wave source and an infinite number of antennas experiencing the same field strength. In actual measurements the THz beam extends only over a limited number of antennas (~9) which will experience various field strengths depending on their location with respect to the profile of the THz beam. That means the observed shape and strength of the transmission resonance is a cumulative effect of several antennas with different resonance shifts which results in a resonance broadening.

From the transmission measurements of the antenna arrays, we find that the minimal peak electric field of the incident THz wave required to observe measurable frequency shift of the resonance is 19 kV cm^{-1} for the

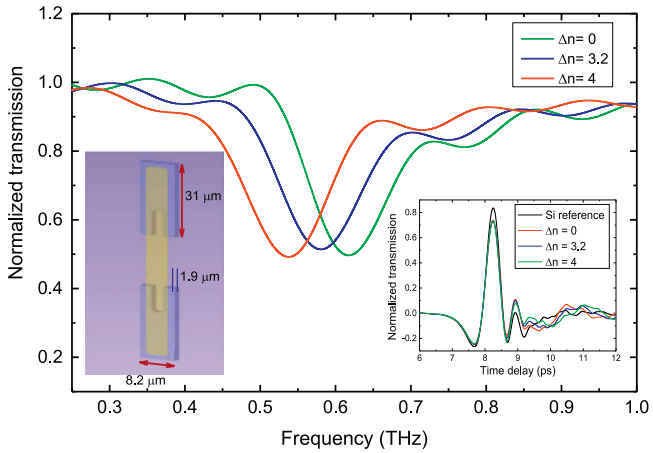

Figure 5. Simulated transmission of an antenna array on HR silicon as function of frequency. Δn is the change in refractive index of the substrate region where the peak field strength is higher than the threshold value E_{th}. The inset on the left shows the local substrate region where index is changed by 4.0. The inset on the right shows the corresponding transmitted THz transient calculated inside the silicon substrate.

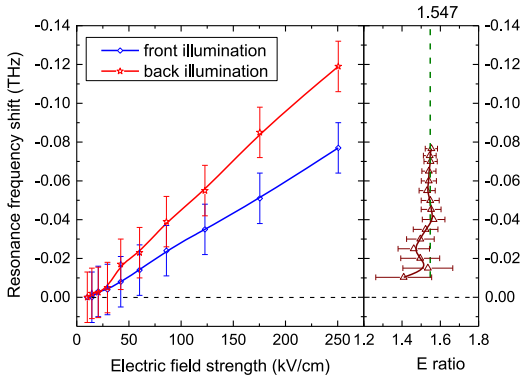

Figure 6. Measured resonance frequency shift of an antenna array as a function of incident THz field strength for front and back illumination. The ratios of field strength that give same resonance shift are shown as triangles on the right. The curves are included for visual aid. The green dashed line indicates the theoretically expected value for HR Si substrate.

front illumination (see figure 6). The numerical simulation results show that the antenna with resonant frequency of 0.6 THz enhances the THz field locally by more than 30 times (time domain enhancement) relative to the input reference field. Thus, the actual local threshold peak electric field strength, E_{th} for resonance frequency shift is estimated to be 570 kV cm^{-1}. This threshold value is used to estimate the region of the substrate near the antenna tips where the refractive index changes. The threshold value is significantly higher than the 200 kV cm^{-1} required for impact ionization in silicon with a static field [38]. We speculate that impact ionization in silicon can still happen in the presence of a THz source with field strength less than 570 kV cm^{-1}. However, the number of carriers can be insufficient and limited only to a small region near the antenna tips to cause an appreciable shift in the resonance frequency of the antenna.

The resonant frequency shift of the antenna array with respect to low THz field strength transmission as a function of incident THz field strength is plotted in figure 6, both for THz transients illuminating the sample from the antenna side (front illumination) and from the substrate side (back illumination). It is apparent that the resonance frequency shift is larger for back illumination than for front illumination for a given incident field strength. The ratio of the field strengths between front illumination and back illumination that result in the same resonance shift is shown in the right panel of figure 6. The measured ratio is consistent with our theoretical prediction presented below.

It is clear from figure 6 that the resonance frequency of the antenna array depends on the direction of illumination of the sample. The increase of the local electric field when illuminated from the substrate side as compared to a direct illumination from the antenna side is somehow counterintuitive. One could at first glance expect that the Fresnel reflection loss on the air-substrate interface $2/(n_{sub} + 1)$, where n_{sub} is the refractive index of the substrate, would reduce the field enhancement in the case of back illumination. But as we show

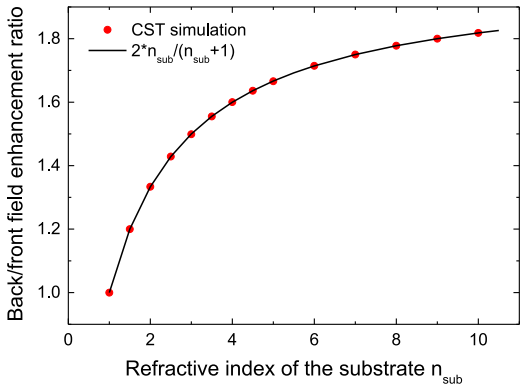

Figure 7. Ratio of the field enhancement at a distance of 1 μm from the tip of the antenna for the back and front illumination.

below other factors provide extra enhancement on the substrate-antenna interface which result in an increase of the local electric field. The observed increase is neither a result of etalon interference effects in the finite thickness substrate (consecutive reflections in the substrate are well separated in time) nor the effect of focusing THz beam into smaller spot inside material with high refractive index (substrate is too thin). In a simple air-dielectric-air configuration electric field on the air side in a close proximity to the surface can be expressed as $E_{\mathrm{air}}^{\mathrm{front}} = E_i + E_r = E_i + E_i(1 - n_{\mathrm{sub}})/(1 + n_{\mathrm{sub}})$ (front illumination) and $E_{\mathrm{air}}^{\mathrm{back}} = E_t = E_i \cdot 4n_{\mathrm{sub}}/(1 + n_{\mathrm{sub}})^2$ (back illumination) where E_i is the incident electric field, E_r is the reflected electric field, and E_t is the transmitted electric field. On the dielectric side of the interface, $E_{\mathrm{sub}}^{\mathrm{front}} = E_t = E_i \cdot 2/(1 + n_{\mathrm{sub}})$ (front illumination), and $E_{\mathrm{sub}}^{\mathrm{back}} = E_t + E_r = E_i[1 - (1 - n_{\mathrm{sub}})/(1 + n_{\mathrm{sub}})] \cdot 2/(1 + n_{\mathrm{sub}})$ (back illumination). Both equations hold as long as the distance to the surface is much shorter than the wavelength inside considered material. In both cases electric field is higher for back illumination with a field ratio of $E_{\mathrm{air}}^{\mathrm{back}}/E_{\mathrm{air}}^{\mathrm{front}} = E_{\mathrm{sub}}^{\mathrm{back}}/E_{\mathrm{sub}}^{\mathrm{front}} = 2n_{\mathrm{sub}}/(n_{\mathrm{sub}} + 1) > 1$.

The presence of metal structures on the substrate complicates the situation somewhat. But consideration of the induced current by the antenna shows that the current in the antenna with back illumination is also enhanced by a factor of $2n_{\mathrm{sub}}/(1 + n_{\mathrm{sub}})$ in comparison to the front illumination as described below. The effective surface current $\vec{J}$ on a dielectric-metal interface can be expressed by $\vec{J} = \vec{n} \times \vec{H}_{\parallel}$ [39]. The current is directly proportional to the magnetic component of the electromagnetic wave parallel to the surface $\vec{H}_{\parallel}$ (the perpendicular component at the metal surface is 0). In case of the perfect electric conductor, $H_{\parallel} = 2H_i$ where H_i is the incident magnetic field. In the dielectric material, $H_i = k_0 \cdot n \cdot E_i$. When the Fresnel reflection loss $2/(1 + n_{\mathrm{sub}})$ at the back substrate is included, we directly see that $J^{\mathrm{back}}/J^{\mathrm{front}} = 2n_{\mathrm{sub}}/(1 + n_{\mathrm{sub}})$.

To verify those analytical predictions we performed a numerical frequency domain simulation of the electric field enhancement in the vicinity of the resonant metal antenna tip for various refractive indices of the substrate for the front and back illumination, see figure 7. It is clear that the simulation result is identical to the theoretical prediction.

The observed refractive index change of the substrate can be explained by field-induced generation of free carriers. We calculated the refractive index of silicon as a function of carrier concentration using the Drude model with parameters reported by Willis *et al* [37]. At a frequency of 0.6 THz (the resonance frequency of the antenna), the local carrier concentration is estimated to be more than 10^{17} cm^{-3} in order to reproduce the refractive index change at an incident THz field of 251 kV cm^{-1}. This is seven orders of magnitude larger than the intrinsic carrier concentration of the undoped HR silicon substrate (1.45×10^{10} cm^{-3} as specified by the supplier). Similar extreme carrier generation induced nonlinearly by an intense THz field is also reported in [40, 41].

To find the main physical mechanism for this very significant carrier generation we have measured the temperature-dependent resonance shift for an antenna array of resonance frequency 0.9 THz. First we vary the incident THz field strength on the sample at temperatures of 10 K and 300 K. The result shows that resonance shift is larger for low temperature at all incident field values as shown in figure 8(a). We also measured the resonance shift as a function of temperature in a range from 10 K to 300 K as shown in figure 8(b). The measurement shows that the resonance shift, which indicates the level of generated carriers, decreases slightly with increasing temperature. Thus, the carrier generation rate reduces at higher temperature.

Two physical processes are known to generate high carrier density in semiconductors, namely Zener tunneling and impact ionization. Zener tunneling is a pronounced phenomenon in direct bandgap semiconductors [42, 43]. Since it is a momentum-conserving process, tunneling occurs between equal wave

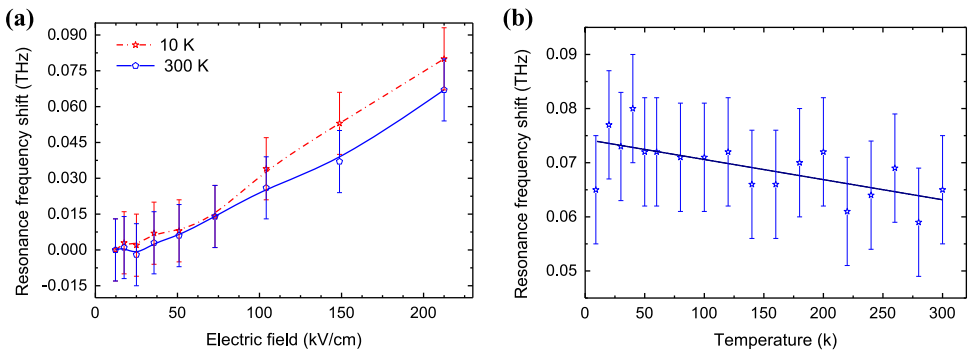

Figure 8. (a) Measured resonance frequency shift of an antenna array as a function of incident THz field strength at temperatures of 10 and 300 K. The blue and the red curves are included for visual aid. (b)The resonance frequency shift of an antenna array as a function of temperature for an incident THz field of 213 kV cm^{-1}. The dark blue line is a linear fit.

vector points. As silicon is an indirect bandgap material, Zener tunneling is strongly quenched and it must involve scattering processes such as phonon scattering that compensates the Γ and X wave vector-mismatch. A phonon-assisted band-to-band tunneling can occur at field strengths much higher than impact ionization threshold [44]. Since the phonon density increases with increasing temperature, the carrier generation rate should be increased at high temperature had Zener tunneling been the dominant mechanism of carrier generation. Moreover, the bandgap of silicon is reduced at high temperature [45] which should additionally increase the tunneling rate. These trends contradict our temperature dependent measurements.

On the other hand, the decrement of THz-induced carrier generation with increasing temperature is in agreement with earlier reports of the temperature dependence of impact ionization rates in silicon [38, 46]. With rise of temperature electron-phonon scattering is enhanced and the population of electrons that can reach the impact ionization threshold energy before electron-phonon scattering is reduced. To roughly approximate the carrier generation rates by impact ionization and phonon-assisted Zener tunneling, we compared carrier generation rates at a representative static electric field of 0.6 MV cm^{-1} reported earlier. The carrier generation rate is in order of 10^{13} cm^{-3} s^{-1} [44] for Zener tunneling and 10^{21} cm^{-3} s^{-1} for impact ionization. The carrier generation rate for impact ionization is estimated from impact ionization rate reported by Grant [38] and a drift velocity reported by Ershov *et al* [46]. Thus, we can identify impact ionization as the main cause of the significant carrier generation that we observe.

Since silicon is an indirect semiconductor, unlike GaAs, impact ionization involves a large momentum change. The need to conserve momentum reduces the probability of impact ionization, which therefore requires a strong electric field. More than 23 impact ionization events are needed to increase the carrier density by seven orders of magnitude as we estimated. We have performed a simplified numerical simulation of electron ballistic acceleration in the presence of THz electric field. Our simulation shows that a single electron can acquire sufficient kinetic energy (1.6 eV) [2, 7] to induce impact ionization much faster than electron scattering time (110 fs) [37]and that the duration of THz pulse is more than sufficient to reach 23 impact ionization events.

4. Conclusion

In summary, a combination of an intense THz field and an additional field enhancement provided by a metal resonant antenna allows operation in a multi-MV cm^{-1} field strength range which results in carrier multiplication by impact ionization in HR silicon. In the presence of an intense THz field the resonance frequency of the metal antenna array redshifts which we attribute to a change in the refractive index of the substrate due to the substantial generation of carriers. The resonance shift of the antenna array is measured for several field strengths in both front and back THz illuminations. We theoretically predict and experimentally show that back illumination (even though counterintuitive) leads to higher field enhancement. We show that this increase of field enhancement in the back illumination depends on the refractive index of the substrate. This explanation of a simple observation shows that the orientation of the sample can be highly beneficial for wide ranges of nonlinear phenomena at interfaces between dielectrics.

Our measurements and simulations show that the free carrier density in HR silicon has increased by more than seven orders of magnitude. The carrier multiplication is induced by a terahertz pulse with a photon energy three orders of magnitude less than the bandgap of silicon. Unlike impact ionization by high static fields, THz engendered impact ionization is a noncontact process that does not require electrodes. To fully understand the

carrier dynamics and ultrafast scattering processes in silicon, THz pump with a delayed THz probe experiments will be essential. Finally, this extraordinary carrier generation phenomenon can be utilized for new silicon functionalities such as ultrafast switching and modulators and has to be accounted for in a wide range of nonlinear phenomena where silicon is used as a substrate.

Acknowledgments

This work has been financially supported by the Danish Research Council for Technology and Production Sciences through the Project HI-TERA and by the Carlsberg Foundation. We acknowledge insightful discussions with Jørn Hvam, DTU Fotonik.

References

[1] Hirori H, Shinokita K, Shirai M, Tani S, Kadoya Y and Tanaka K 2011 Extraordinary carrier multiplication gated by a picosecond electric field pulse *Nat. Commun.* **2** 594
[2] Sano N and Yoshii A 1992 Impact-ionization theory consistent with a realistic band structure of silicon *Phys. Rev.* B **45** 8
[3] Maes W, De Meyer K and Van Overstraeten R 1990 Impact ionization in silicon: a review and update *Solid State Electron* **33** 705–18
[4] Hoffmann M, Hebling J, Hwang H, Yeh K-L and Nelson K 2009 Impact ionization in InSb probed by terahertz pump—terahertz probe spectroscopy *Phys. Rev.* B **79** 161201 (R)
[5] Tang J Y and Hess K 1983 Impact ionization of electrons in silicon (steady state) *J. Appl. Phys.* **54** 5139–44
[6] Pacelli A, Spinelli A S and Lacaita A L 1998 Impact ionization in silicon: a microscopic view *J. Appl. Phys.* **83** 4760–4
[7] Cartier E, Fischetti M V, Eklund E A and McFeely F R 1993 Impact ionization in silicon *Appl. Phys. Lett.* **62** 3339–41
[8] Clough B, Dai J and Zhang X-C 2012 Laser air photonics: beyond the terahertz gap *Mater. Today* **15** 50–8
[9] Iwaszczuk K, Andryieuski A, Lavrinenko A, Zhang X and Jepsen P U 2012 Terahertz field enhancement to the MV/cm regime in a tapered parallel plate waveguide *Opt. Express* **20** 1289–95
[10] Hirori H, Doi A, Blanchard F and Tanaka K 2011 Single-cycle THz pulses with amplitudes exceeding 1 MV/cm generated by optical rectification in $LiNbO_3$ *Appl. Phys. Lett.* **98** 091106
[11] Hauri C P, Ruchert C, Vicario C and Ardana F 2011 Strong-field single-cycle THz pulses generated in an organic crystal *Appl. Phys. Lett.* **99** 2013–6
[12] Ruchert C, Vicario C and Hauri C P 2012 Scaling submillimeter single-cycle transients toward megavolts per centimeter field strength via optical rectification in the organic crystal OH1 *Opt. Lett.* **37** 899
[13] Vicario C, Monoszlai B and Hauri C P 2014 GV/m single-cycle terahertz fields from a laser-driven large-size partitioned organic crystal *Phys. Rev. Lett.* **112** 1–5
[14] Shalaby M and Hauri C P 2015 Demonstration of a low-frequency three-dimensional terahertz bullet with extreme brightness *Nat. Commun.* **6** 1–8
[15] Beard M, Turner G and Schmuttenmaer C 2000 Transient photoconductivity in GaAs as measured by time-resolved terahertz spectroscopy *Phys. Rev.* B **62** 15764–77
[16] Fan K, Hwang H Y, Liu M, Strikwerda A C, Sternbach A, Zhang J, Zhao X, Zhang X, Nelson K A and Averitt R D 2013 Nonlinear terahertz metamaterials via field-enhanced carrier dynamics in GaAs *Phys. Rev. Lett.* **110** 217404
[17] Hebling J, Yeh K-L, Hoffmann M C, Bartal B and Nelson K A 2008 Generation of high-power terahertz pulses by tilted-pulse-front excitation and their application possibilities *J. Opt. Soc. Am.* B **25** B6
[18] Beaudoin A, Salem B, Baron T, Gentile P and Morris D 2014 Impact of n-type doping on the carrier dynamics of silicon nanowires studied using optical-pump terahertz-probe spectroscopy *Phys. Rev.* B **89** 115316
[19] Liu M *et al* 2012 Terahertz-field-induced insulator-to-metal transition in vanadium dioxide metamaterial *Nature* **487** 345–8
[20] Hoi I-C and Zhang X-C 2014 Application of broadband terahertz spectroscopy in semiconductor nonlinear dynamics *Front. Optoelectron.* **7** 220–42
[21] Kane E O 1966 Band structure of silicon from an adjusted Heine–Abarenkov calculation *Phys. Rev.* **146** 8
[22] Al-Naib I, Sharma G, Dignam M M, Hafez H, Ibrahim A, Cooke D G, Ozaki T and Morandotti R 2013 Effect of local field enhancement on the nonlinear terahertz response of a silicon-based metamaterial *Phys. Rev.* B **88** 195203
[23] Iwaszczuk K, Zalkovskij M, Strikwerda A C and Jepsen P U 2015 Nitrogen plasma formation through terahertz-induced ultrafast electron field emission *Optica* **2** 116–23
[24] Strikwerda A C, Iwaszczuk K, Salkovskij M and Jepsen P U Permanently reconfigured metamaterials due to THz induced mass transfer of gold *Rev. Opt. Express* under revision
[25] Yoshioka K, Minami Y, Shudo K-I, Dao T D, Nagao T, Kitajima M, Takeda J and Katayama I 2015 Terahertz-field-induced nonlinear electron delocalization in Au nanostructures *Nano Lett.* accepted
[26] Hebling J, Almasi G, Kozma I and Kuhl J 2002 Velocity matching by pulse front tilting for large area THz-pulse generation *Opt. Express* **10** 1161–6
[27] Fülöp J A, Pálfalvi L, Almási G and Hebling J 2010 Design of high-energy terahertz sources based on optical rectification *Opt. Express* **18** 12311–27
[28] Hirori H, Doi A, Blanchard F and Tanaka K 2011 Single-cycle terahertz pulses with amplitudes exceeding 1 MV/cm generated by optical rectification in $LiNbO_3$ *Appl. Phys. Lett.* **98** 091106
[29] Winnewisser C, Jepsen P U, Schall M, Schyja V and Helm H 1997 Electro-optic detection of THz radiation in $LiTaO_3$, $LiNbO_3$ and ZnTe *Appl. Phys. Lett.* **70** 3069
[30] Wu Q, Litz M and Zhang X-C 1996 Broadband detection capability of ZnTe electro-optic field detectors *Appl. Phys. Lett.* **68** 2924
[31] Nahata A, Auston D H, Heinz T F and Wu C 1996 Coherent detection of freely propagating terahertz radiation by electro-optic sampling *Appl. Phys. Lett.* **68** 150
[32] Ku S A, Tu C M, Chu W, Luo C W, Wu K H, Yabushita A, Chi C C and Kobayashi T 2013 Saturation of the free carrier absorption in ZnTe crystals *Opt. Express* **21** 13930–7

[33] Tian Z, Wang C, Xing Q, Gu J, Li Y, He M, Chai L, Wang Q and Zhang W 2008 Quantitative analysis of Kerr nonlinearity and Kerr-like nonlinearity induced via terahertz generation in ZnTe *Appl. Phys. Lett.* **92** 041106
[34] Crozier K B, Sundaramurthy A, Kino G S and Quate C F 2003 Optical antennas: resonators for local field enhancement *J. Appl. Phys.* **94** 4632
[35] Werley C A, Fan K, Strikwerda A C, Teo S M, Zhang X, Averitt R D and Nelson K A 2012 Time-resolved imaging of near-fields in THz antennas and direct quantitative measurement of field enhancements *Opt. Express* **20** 8551–67
[36] Dai J, Zhang J, Zhang W and Grischkowsky D 2004 Terahertz time-domain spectroscopy characterization of the far-infrared absorption and index of refraction of high-resistivity, float-zone silicon *J. Opt. Soc. Am.* B **21** 1379
[37] Willis K J, Hagness S C and Knezevic I 2013 A generalized Drude model for doped silicon at terahertz frequencies derived from microscopic transport simulation *Appl. Phys. Lett.* **102** 122113
[38] Grant W N 1973 Electron and hole ionization rates epitaxial silicon at high electric fields *Solid State Electron* **16** 1189–203
[39] Jackson J D 1999 *Classical Electrodynamics* 3rd edn (New York: Wiley) p 832
[40] Jeong Y G, Paul M J, Kim S H, Yee K J, Kim D S and Lee Y S 2013 Large enhancement of nonlinear terahertz absorption in intrinsic GaAs by plasmonic nano antennas *Appl. Phys. Lett.* **103** 28–31
[41] Lange C, Maag T, Hohenleutner M, Baierl S, Schubert O, Edwards E R J, Bougeard D, Woltersdorf G and Huber R 2014 Extremely nonperturbative nonlinearities in GaAs driven by atomically strong terahertz fields in gold metamaterials *Phys. Rev. Lett.* **113** 227401
[42] Di Carlo A, Lugli P and Vogl P 1997 Enhanced Zenner tunneling in silicon *Solid State Commun.* **101** 921–3
[43] Quade W, Scholl E, Rossi F and Jacoboni C 1994 Quantum theory of impact ionization in coherent high-field simiconductor transport *Phys. Rev.* B **50** 7398–412
[44] Schenk A 1993 Rigorous theory and simplified model of the band-to-band tunneling in silicon *Solid State Electron* **36** 19–34
[45] Bludau W, Onton A and Heinke W 1974 Temperature dependence of the band gap of silicon *J. Appl. Phys.* **45** 1846
[46] Ershov M and Ryzhii V 1995 Temperature dependence of the electron impact ionization coefficient in silicon *Semicond. Sci. Technol.* **10** 138–42